JOURNAL OF AIRCRAFT
Vol. 42, No. 5, September–October 2005

Aerodynamic Active Control for Fin-Buffet Load Alleviation

Christian Breitsamter*
Technische Universität München, 85747 Garching, Germany

The efficiency of an active auxiliary rudder system in alleviating fin buffeting of modern fighter aircraft is investigated. Low-speed wind-tunnel tests are performed on a detailed 1/15-scale model of canard-delta-wing type. A digitally controlled auxiliary rudder is installed on a specific fin model providing harmonic oscillations at varying frequency and deflection angle. The vertical tail is instrumented to measure unsteady surface pressures, fin-tip accelerations, and auxiliary rudder moments. At open-loop tests the fin unsteady pressure field is fed with energy at the frequencies of the auxiliary rudder motions. The corresponding rms values increase with increasing frequency and deflection angle at all angles of attack tested. The motion-induced rms pressures reach values well above the levels of the nonoscillating case. Thus, a potential to reduce rms buffet loads by approximately 18% for closed-loop operations exists. There is no decrease in the rudder moment with increasing angle of attack substantiating the effectiveness of the auxiliary rudder concept also for high angles of attack. The active control system uses single-input single-output control laws to alleviate buffeting in the fin first bending and torsion mode, respectively. With active control the spectral density peaks of fin-tip accelerations at the frequencies of the considered eigenmodes can be reduced by as much as 60% at angles of attack up to 31 deg.

Nomenclature

A_{F_T}	=	surface area of auxiliary rudder, 0.02941 m^2
c_M	=	moment coefficient
$c_p(t)$	=	pressure coefficient, $[p(t) - p_\infty]/q_\infty$
$\bar{c}_p$	=	time-averaged pressure coefficient
c'_p	=	fluctuation part of c_p
$\hat{c}_p$	=	amplitude spectrum of pressure coefficient, $\sqrt{(2S_{c_p}\Delta k U_\infty / l_\mu)}$
$c_{p_{\text{rms}}}$	=	rms value of c'_p, $\sqrt{(\overline{c'^2_p})}$
f	=	frequency, Hz
g	=	gravitational acceleration, 9.81 m/s^2
K_p	=	controller gain parameter, deg/g
k	=	reduced frequency, $f l_\mu / U_\infty$
l_μ	=	wing mean aerodynamic chord, m
M_{ζ_T}	=	auxiliary rudder moment, Nm
$p(t)$, p_∞	=	pressure, ambient pressure, Pa
q_∞	=	freestream dynamic pressure, Pa
Re_{l_μ}	=	Reynolds number, $U_\infty l_\mu / \nu$
S_{c_p}	=	pressure spectral density, 1/Hz
$S_{F_{\ddot{y}}}$	=	normalized power spectral density of fin tip accelerations
s, s_F	=	wing half-span, fin span, m
s_{F_T}	=	span of auxiliary rudder, 0.0656 m
T_1	=	controller time constant, s
t	=	time, s
U_∞	=	freestream velocity, m/s
v'	=	lateral velocity fluctuations, m/s
v_{rms}	=	rms value of v', $\sqrt{(\overline{v'^2})}$, m/s
$\ddot{y}_F(t)$	=	fin-tip accelerations, m/s^2
x_F, y_F, z_F	=	fin coordinates, m
α	=	aircraft angle of attack, deg
β	=	aircraft angle of sideslip, deg
Λ	=	aspect ratio
λ	=	taper ratio
ν	=	kinematic viscosity, m^2/s
φ	=	leading-edge sweep, deg
Φ	=	phase angle, deg

Subscripts

C, W, F	=	canard, wing, fin
dom	=	dominant
ζ_T	=	auxiliary rudder

Introduction

MODERN fighter aircraft are subject to high-angle-of-attack maneuvers extending the flight envelope to the stall and post-stall regime.[1] Slender wing geometries, for example, delta-wing planforms, strakes, and leading-edge extensions, respectively, are used to generate strong large-scale vortices shed at the highly swept leading edges. The leading-edge vortices improve significantly the high-α performance because of additional lift and an increase in maximum angle of attack. At high angle of attack, however, the leading-edge vortices burst already over the wing planform. The transition from stable to unstable core flow, evident by the rapid change in the axial velocity profiles from jet type to wake type, leads to extremely high turbulence intensities at the breakdown position and to increased turbulence levels further downstream.[2] Hence, the buffet excitation level increases strongly above a certain angle of attack, and fin normal force spectra are characterized by narrowband peaked distributions. Such unsteady aerodynamic loads often excite the vertical tail structure in its natural frequencies resulting in increased fatigue loads, reduced service life, and raised maintenance costs.[3]

The fin buffeting problem plagues twin-fin configurations (F-15, F/A-18), but single-fin aircraft are also affected.[3,4] Therefore, comprehensive research programs have been undertaken aimed at understanding the buffet loads and reducing the structural response. The related vortical flow features are carefully analyzed using wind-tunnel tests on small-scale and full-scale models,[5–7] supplemented by flight tests,[8] and detailed numerical flow simulations.[9,10] In addition, design methods have been developed by Zimmerman et al. and Ferman et al. to describe the fin buffet environment and to predict buffet loads for use in aircraft design.[11,12]

To improve the knowledge on the flow physics associated with fin buffeting, extensive experiments on the low-speed fin flow environment of a modern fighter aircraft model have been conducted at the Institute for Fluid Mechanics (FLM) of the Technische Universität München (TUM).[2,13] The studies focus on the turbulent flow structure well defined by the spatial and temporal characteristics of the

Received 9 February 2004; revision received 24 May 2004; accepted for publication 25 May 2004.

*Dr.-Ing., Chief Scientist, Aerodynamics Division, Institute for Fluid Mechanics. Senior Member AIAA.

unsteady flow velocities. It was found that the flow downstream of bursting is subject to a helical mode instability. The quasi-periodic velocity fluctuations associated with the most unstable normal mode of the mean axial velocity profile of the burst vortex core evoke coherent unsteady surface pressures (buffet).[2] Downstream of bursting, maximum turbulence intensities are concentrated on a limited radial range related to the points of inflection in the radial profiles of the retarded axial core velocity. The flowfields show that with increasing incidence the burst vortex cores grow significantly moving inboard and upward. Consequently, a centerline fin can also encounter high turbulence levels in the high-α regime.[13] Further, the turbulence intensities in the fin region can increase markedly for some sideslip reaching levels typically obtained at twin-fin stations where the fin is directly enveloped by the breakdown flow.[14]

The buffet loads do not only decrease the fatigue life of the airframe, but can, in turn, limit the angle-of-attack envelope of the aircraft. To counter the fin-buffeting problem, several methods have been suggested. They deal with alterations of the fin structural properties like stiffness and damping,[15] aerodynamic modifications for a passive or active control of vortex trajectories to avoid a direct impact of the burst vortical flow on the fin,[16] and methods of active vibration control.[17–20] With active control the structural dynamic loads are reduced aimed both to increase the service live and to improve the maneuverability by extending the angle-of-attack envelope (Fig. 1). For active vibration alleviation various actuators have been discussed and tested involving both structural and aerodynamic concepts. The structural methods focus mainly on surface-integrated piezoactuators or on a piezointerface between the fin and fuselage structure.[18–21] In the aerodyamic field, a tip vane, a rotating or oscillating slotted cylinder mounted at the fin tip, and an active rudder are studied.[17,19,20] Considering the moving vane or slotted cylinder, the motion-induced aerodynamic forces might be too small to damp effectively the buffet-induced vibrations. The rudder might work more efficiently, but its mass hampers high-frequency operations restricting the damping of structural vibrations usually to the fin first bending mode.[17] In addition, aircraft handling qualities could be affected. Recently, comprehensive investigations on active fin-buffet load alleviation have been performed on the F/A-18 full-scale vertical tail applying advanced distributed piezoelectric actuators, feedback control of the rudder, switch mode amplifiers, and advanced control strategies. Consequently, the enhanced performance and capability of new technology active buffet suppression systems are demonstrated.[22–25]

Here, an active auxiliary rudder is proposed using the upper part of a standard rudder for adaptive vibration control. The experiments presented concentrate on the efficiency of the auxiliary rudder concept, which is tested the first time on an EF-2000 type wind-tunnel model.[26]

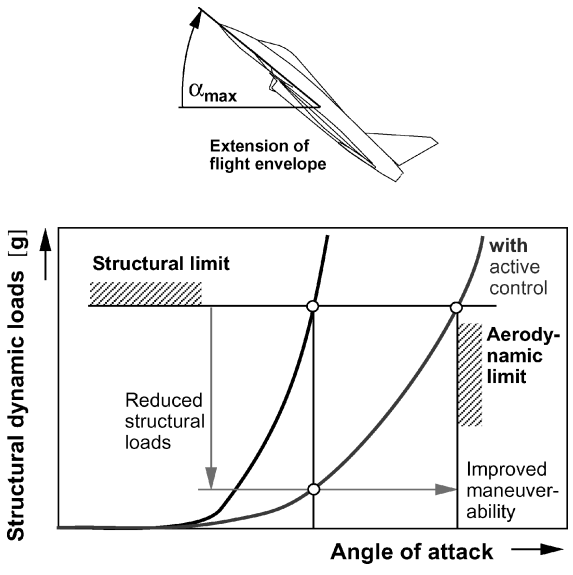

Fig. 1 Increase in performance by active buffet load alleviation.

Experimental Technique

Model and Facility

For the tests a detailed steel model of a modern fighter aircraft of canard-delta-wing type is used. The model consists of nose section, front fuselage with rotatable canards and a single place canopy, center fuselage with delta-wing section and a through-flow double air intake underneath, and rear fuselage including nozzle section and the vertical tail (fin) (Fig. 2). For the experiments reported herein the existing vertical tail was replaced by a newly constructed fin equipped with an actively controlled auxiliary rudder. Geometry and main assembly parts are shown in Fig. 3. The fin is flexible and was scaled to match the reduced frequency of the actual aircraft. The scaling is shown in the following section.

The manufactured parts include the fin with instrumentation cover, the auxiliary rudder, the body insert to fasten the fin to the rear fuselage, and the driving components. The auxiliary rudder is commanded via an excenter gear by a computer-controlled servomotor providing harmonic rudder motions (Fig. 4). The oscillation frequency f_{ζ_T} can be adjusted digitally at a maximum rudder deflection angle of $\zeta_{T_{\max}} = 1, 3, 5$ deg. The fin is instrumented with two tip accelerometers, 18 differential unsteady pressure transducers at nine positions directly opposite each other on each surface, and a torque moment transducer at the driven rudder shaft (Fig. 4).

The investigations are carried out in the Göttingen-type low-speed wind-tunnel facility B of the FLM (Aerodynamics Division) of the TUM. The open test section is 1.2 m in height, 1.55 m in width, and 2.8 m long. Maximum usable velocity is 60 m/s at a turbulence level less than 0.4%. The model is sting mounted in the open test section using a computer-controlled three-axis model support (Fig. 5).

Test Conditions and Measured Quantities

Because active control of buffet-induced vibrations is the primary focus, the fin first bending and torsion modes are of particular interest. At wind-off the first bending mode of the fin model is around 145 Hz, and the first torsion mode is around 387 Hz. The structural damping is about 4.4%, whereas the aerodynamic damping is 3.2 to 4.8% for $\alpha = 25$ to 31.2 deg.

$2s = 0.740$ m	$\varphi_W = 50°$
$l_\mu = 0.360$ m	$\varphi_C = 45°$
$\Lambda_W = 2.45$	$\lambda_W = 0.14$

$s_F = 0.47\ s$	$\varphi_F = 54°$
$\Lambda_F = 1.38$	$\lambda_F = 0.19$

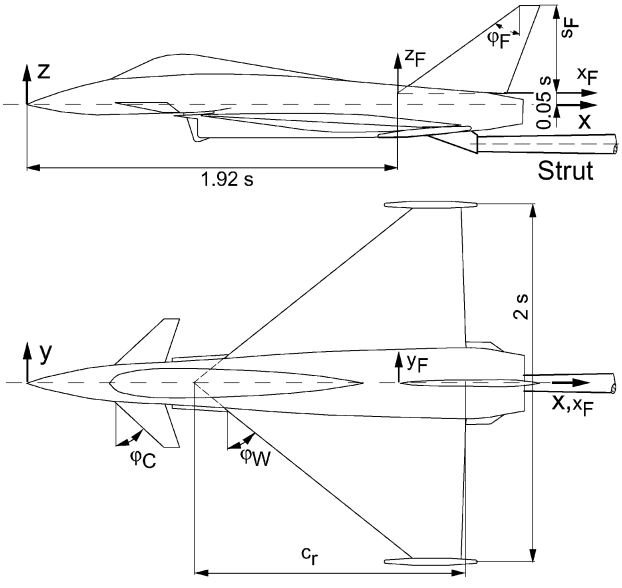

Fig. 2 Geometry of delta-canard wind-tunnel model.

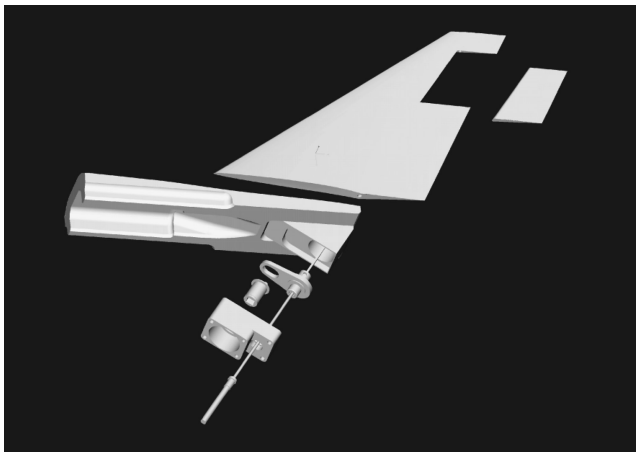

a)

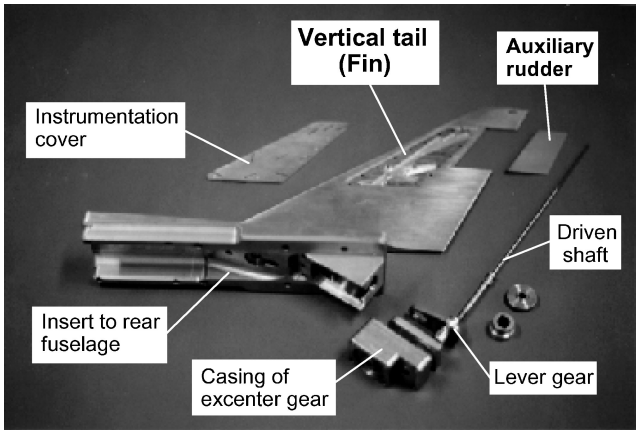

b)

Fig. 3 CAD and manufactured parts of the model fin section including the active auxiliary rudder: a) CAD model of fin section and b) assembly components of fin section.

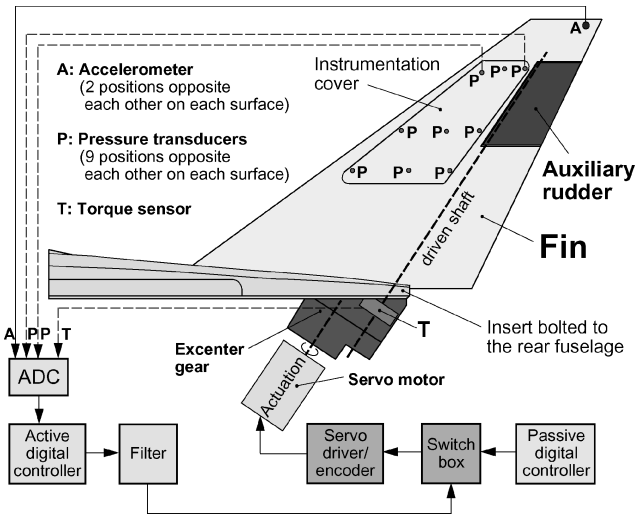

Fig. 4 Integrated measurement and control system for active buffet load alleviation.

For buffet, the reduced frequency k with

$$fl_\mu/U_\infty = f_M l_{\mu_M} \big/ U_{\infty_M} \qquad \text{M: Model} \qquad (1)$$

is the basic similarity parameter in determining test conditions.[11,19] The corresponding frequency ratio between the structural modes of an actual aircraft and the model is about 1/8. The model scale is 1/15. Regarding low-speed, high-angle-of-attack maneuvers the

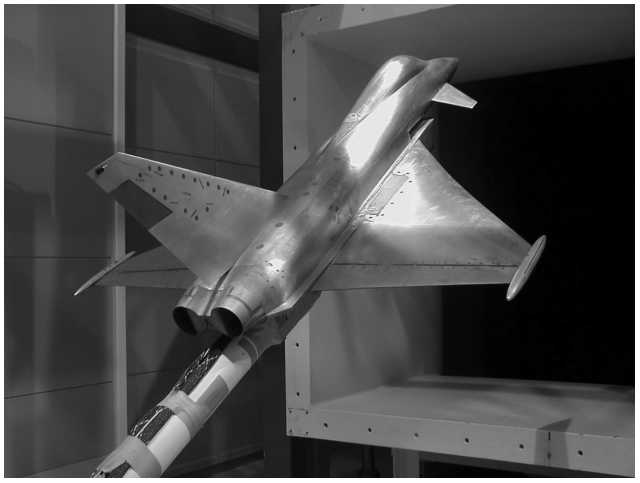

a)

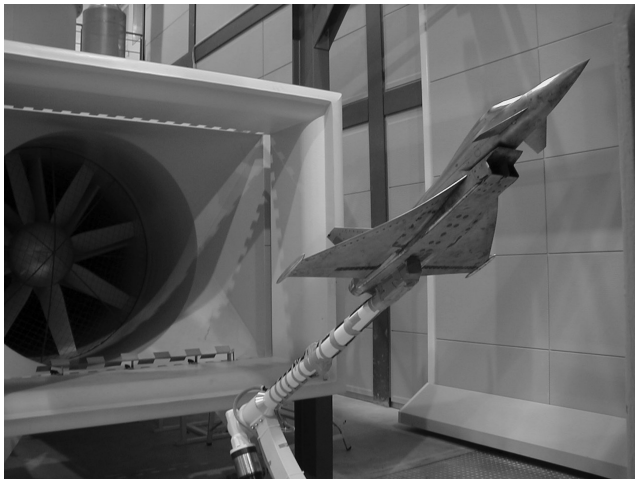

b)

Fig. 5 Views of 1/15-scale delta canard model mounted in test section of FLM low-speed wind tunnel B: a) rear view and b) front view.

tests are made at a freestream reference velocity of $U_\infty = 40$ m/s corresponding to a Reynolds number of $Re_{l_\mu} = 0.97 \times 10^6$ based on the wing mean aerodynamic chord. The angle of attack is varied in the range of 0 deg $\leq \alpha \leq$ 31.2 deg at sideslip angles of $\beta = 0$ and 5 deg. The results presented focus on symmetric freestream. At all experiments turbulent boundary layers exist at wing and control surfaces known from previous measurements.[2]

Using a multichannel data-acquisition system, voltages of unsteady surface-pressure transducers, fin-tip accelerometers, and rudder moment sensor are amplified for optimal signal levels, low-pass filtered at 256 and 1000 Hz, respectively, simultaneously sampled and digitized with 14-bit precision. The sampling frequency for each channel is set to 2000 Hz, and the sampling interval is 30 s. Data-acquisition parameters are based on preliminary tests to cover all significant flow phenomena as well as on statistical accuracies of 1, and 2.5% for the rms values and spectral densities, respectively.[2,26]

Buffet and Buffeting Characteristics

At the FLM comprehensive studies on the vortical flowfields associated with fin buffeting have been conducted on generic models as well as on the EF-2000 type model.[13,14] The impact of the flowfield on the fin structure can be characterized by the lateral rms velocities surveyed carefully within the fin region. Summarizing, the rms values for different vertical fin stations are shown as function of angle of attack in Fig. 6a. The magnitude of the rms values in the midsection depends on the development of the vortical

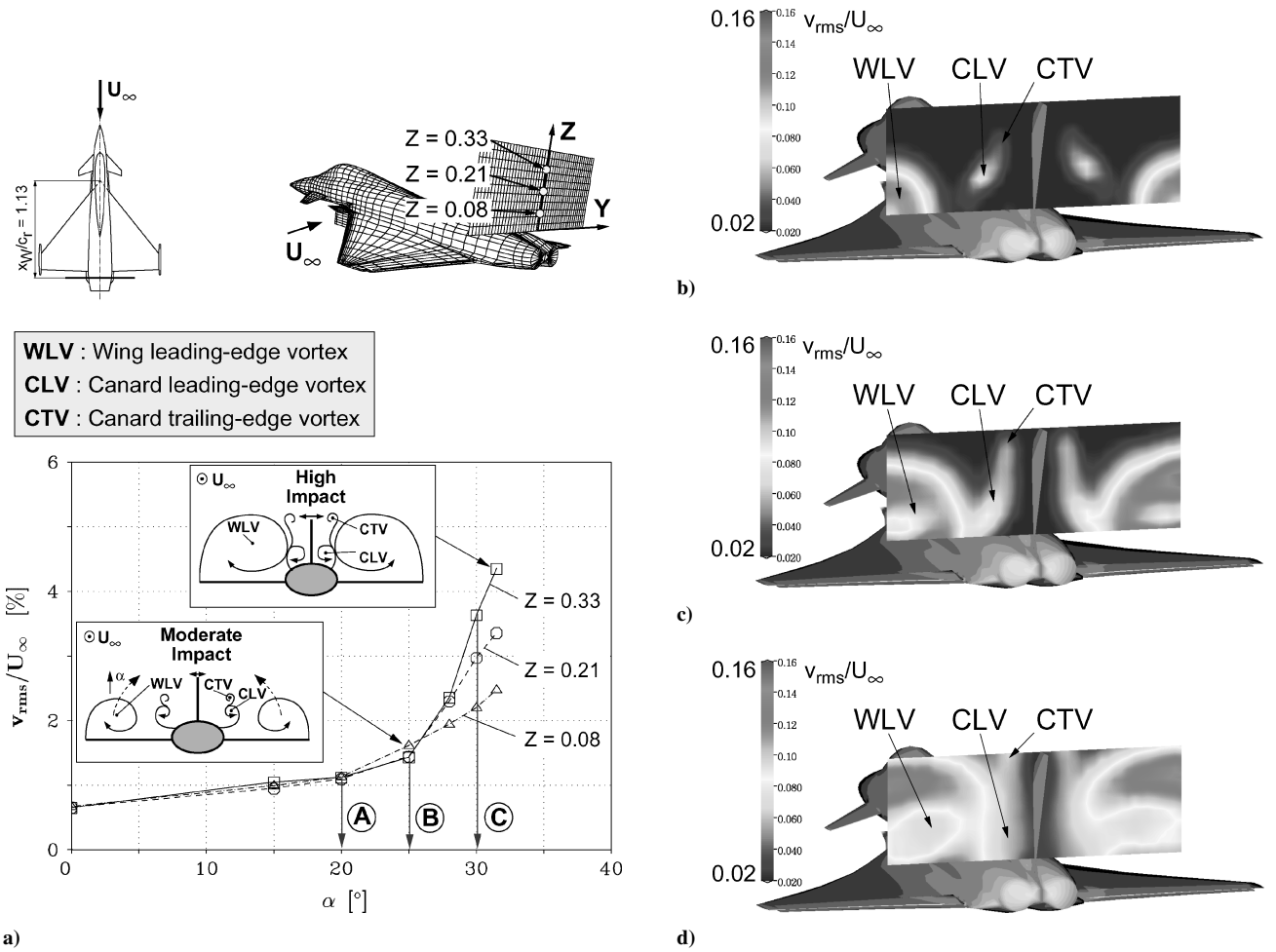

Fig. 6 Lateral rms velocities v_{rms}/U_∞ measured in the fin region and in a plane normal to the fin surface for various angles of attack, where $U_\infty = 40$ m/s, $Re_{l_\mu} = 0.97 \times 10^6$, and $\beta = 0$ deg: a) rms values for different vertical fin stations Z and rms crossflow patterns at b) $\alpha = 20$ deg, c) $\alpha = 25$ deg, and d) $\alpha = 30$ deg.

flow structure. This is depicted by the schematics of Fig. 6a, which are based on the rms velocity patterns in planes normal to the fin surface (Figs. 6b–6d). At moderate angles of attack, the area of the centerline fin is only a little affected by the regions of highly turbulent flow because of the burst wing leading-edge vortices (WLVs) and canard leading-edge vortices (CLVs) and trailing-edge vortices (CTVs) (Fig. 6b). Above $\alpha = 25$ deg, the lateral turbulence intensities in the fin region increase significantly with increasing angle of attack as the burst WLVs expand and approach the mid section (Fig. 6c). Also the CLVs and CTVs come close to the midsection. In particular, the fin flow is influenced by induction effects arising from the WLV vortex sheets, which are the loci of maximum turbulence intensity. The interaction between WLVs and canard vortices (CLVs and CTVs) leads to local rms maxima within the fin area (Fig. 6d).

The corresponding surface-pressure fluctuations defining the buffet situation are averaged for each side of the fin and plotted together as function of angle of attack (Fig. 7). The buffet pressures increase severely above $\alpha = 25$ deg, reflecting the rise in the lateral rms velocities. The results are taken from different unsteady pressure measurements on the 1/15-scale model (Refs. 2 and 26), as well as from pressure calculations based on measured turbulent flowfields.[14] The data obtained show very good agreement over the considered incidence range.

For further analysis, buffet and buffeting are quantified by nondimensional spectral functions. The amplitude spectra of the buffet pressures show that turbulent energy is channeled into a narrowband (Fig. 8). This spectral energy concentration is detected the first time at $\alpha \approx 22$ deg. At this α, the helical mode instability of the burst WLVs starts to affect the fin pressure field. From $\alpha = 24$ to 31.2 deg the narrowband amplitude increases while the corresponding (dominant) reduced frequency k_{dom} is shifted to lower values. This frequency shift is caused by an increase in the wavelength of the helical mode instability with increasing angle of attack. As demonstrated in Fig. 9, a scaling with the sinus of α and the local wing half-span $x \cdot \cot\varphi_W$ gives an approximately constant value of

$$k_{\text{dom}} \sin\alpha \cot\varphi_W \approx 0.282 \pm 0.025 \tag{2}$$

The pressure distributions discussed (Figs. 7–9) create the buffeting, or structural response to the buffet, typically quantified by power spectral densities (PSDs) of the fin-tip accelerations (Fig. 10). The resulting fin buffeting mainly consists of a response in the first bending mode. Regarding the buffet characteristics at high α along with the fin model used, the dominant buffet frequency comes close to a value half of the bending eigenfrequency, which is then strongly excited, whereas the first torsion mode with a multiple higher eigenfrequency is less excited.

Open-Loop Tests and System Identification

Harmonic (sinusoidal) motions of the auxiliary rudder are performed at various frequencies f_{ζ_T} and maximum deflection angles $\zeta_{T_{\max}}$ of 1, 3, and 5 deg to assess the auxiliary rudder efficiency in altering buffet and buffeting. Compared to the results of the fixed

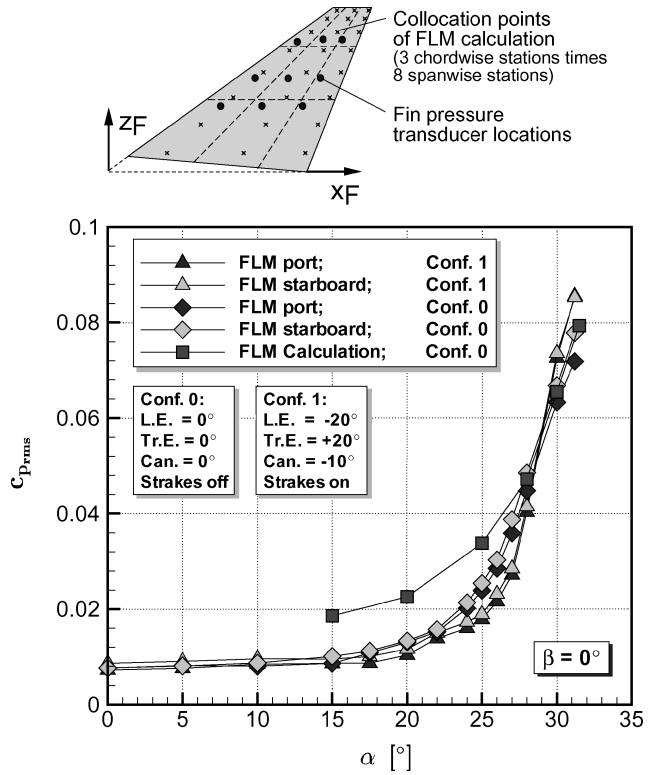

Fig. 7 Measured and calculated fin buffet pressures as function of angle of attack. $Re_{l_\mu} = 0.97 \times 10^6$.

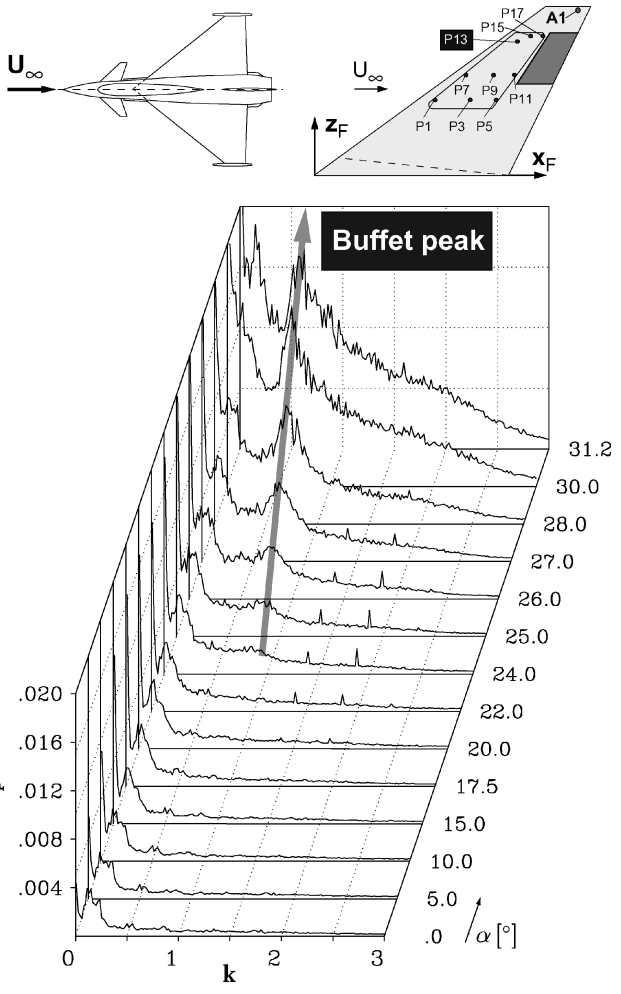

Fig. 8 Amplitude pressure spectra $\hat{c}_p$ taken at station P13 for all angles of attack tested: $U_\infty = 40$ m/s, $Re_{l_\mu} = 0.97 \times 10^6$, and $\beta = 0$ deg.

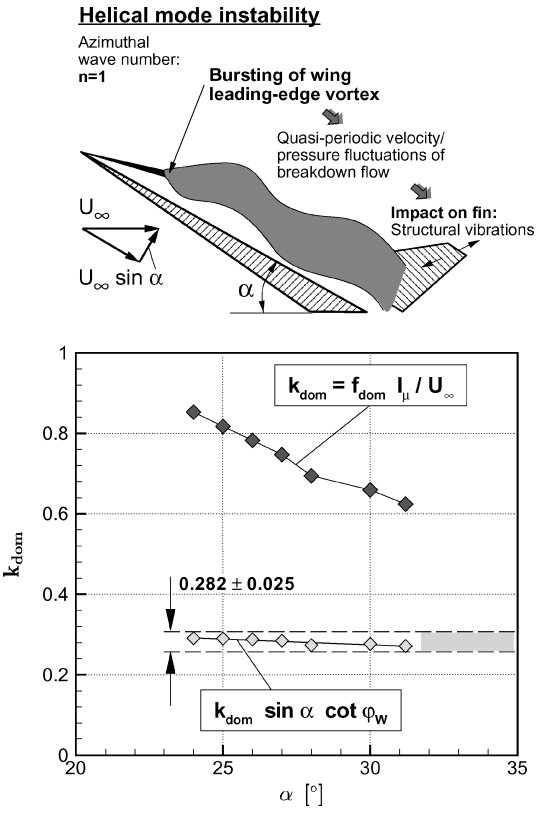

Fig. 9 Dominant reduced buffet frequency k_{dom} as function of angle of attack based on amplitude pressure spectra of fin station P13.

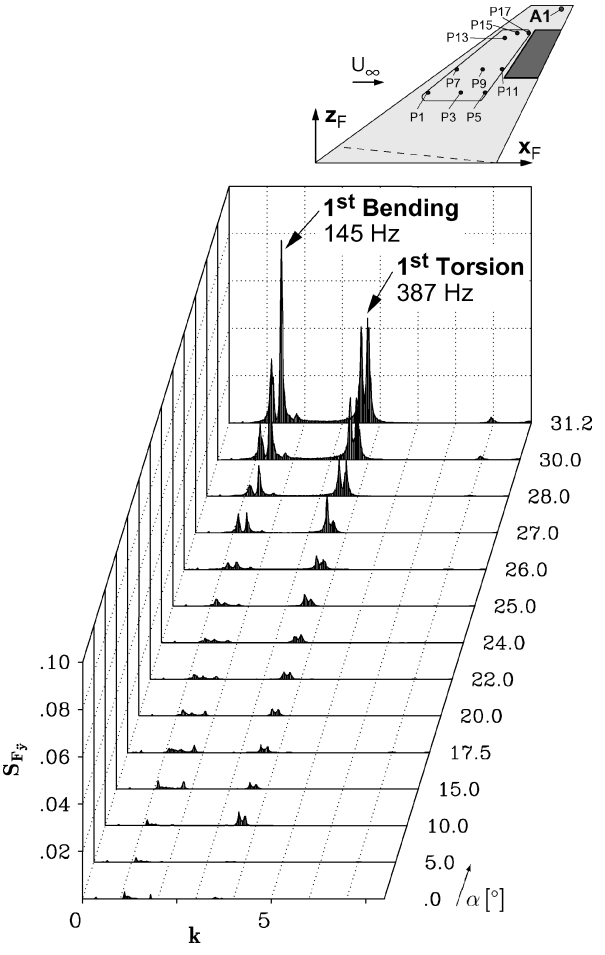

Fig. 10 PSDs of fin-tip accelerations $S_{F_{\ddot{y}}}$ taken at station A1 for all angles of attack tested: $U_\infty = 40$ m/s, $Re_{l_\mu} = 0.97 \times 10^6$, and $\beta = 0$ deg.

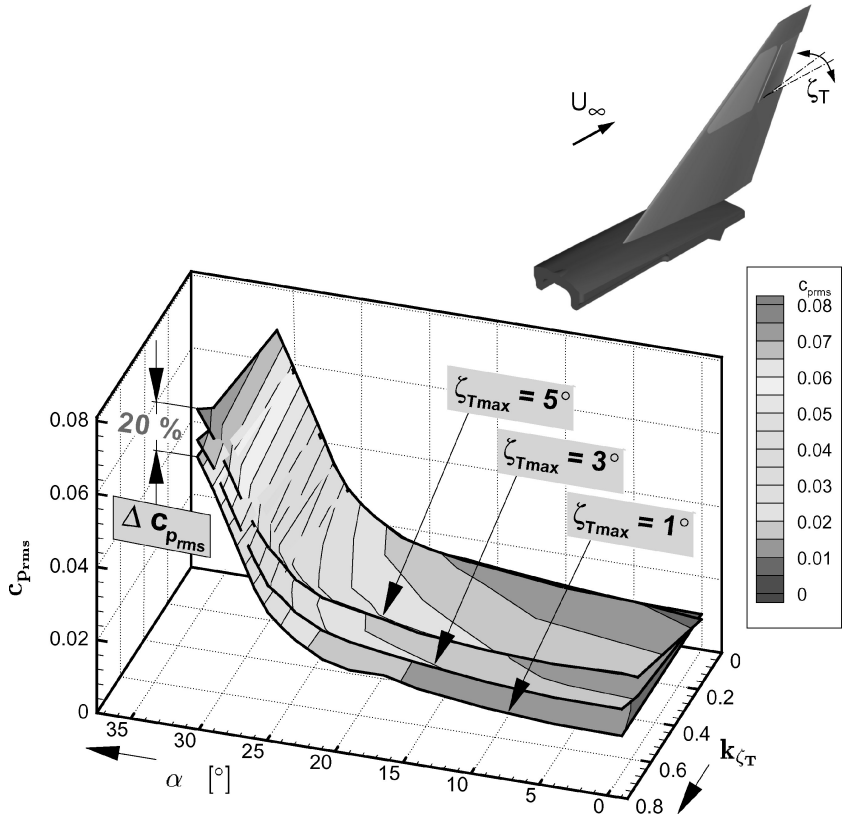

Fig. 11 Surface-averaged rms pressures $c_{p_{\mathrm{rms}}}$ of fin starboard side as function of angle of attack α, reduced auxiliary rudder frequency k_{ζ_T}, and rudder deflection angle $\zeta_{T_{\max}}$: $U_\infty = 40$ m/s, $Re_{l_\mu} = 0.97 \times 10^6$, and $\beta = 0$ deg.

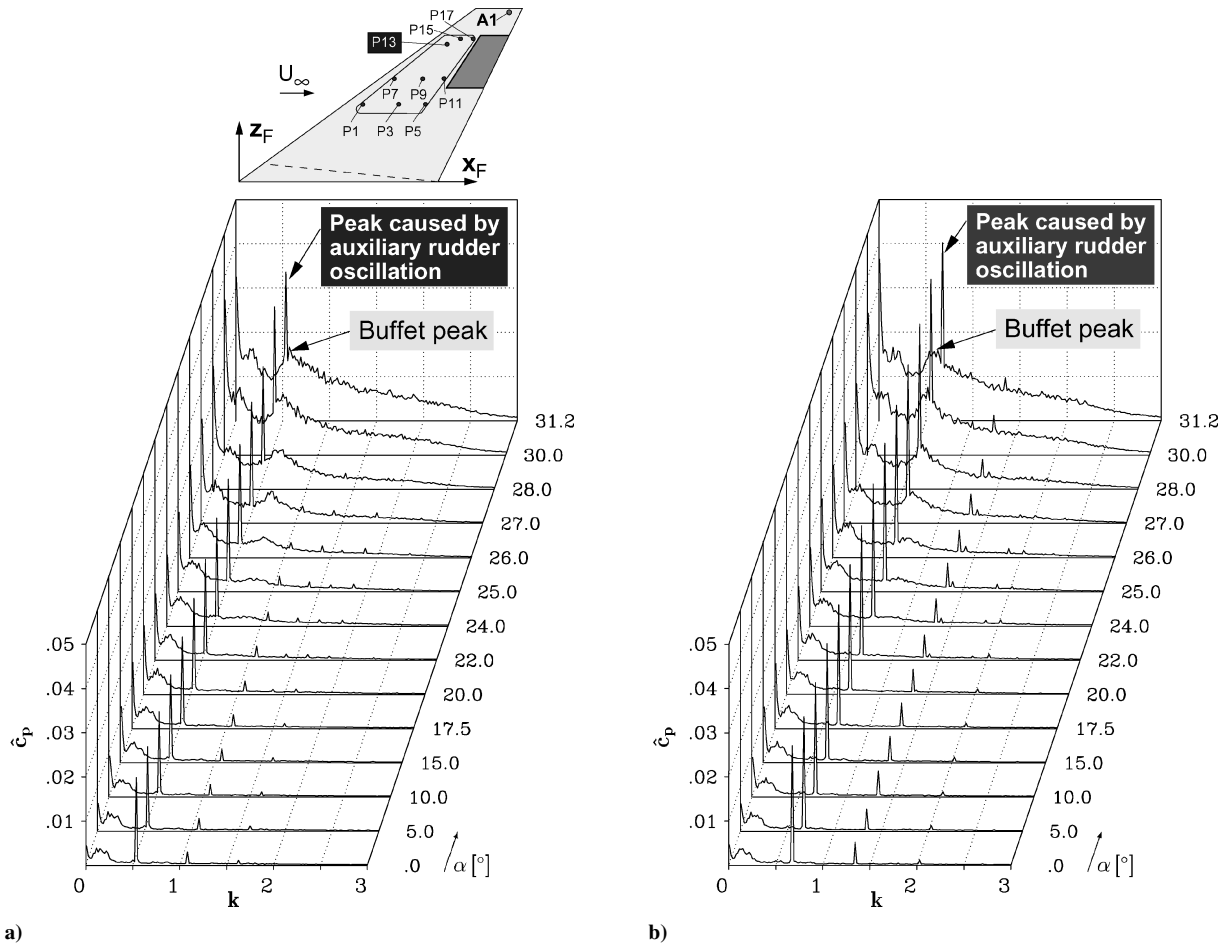

Fig. 12 Amplitude spectra of fin pressure fluctuations $\hat{c}_p$ at station P13 for all angles of attack tested, where $U_\infty = 40$ m/s, $Re_{l_\mu} = 0.97 \times 10^6$, and $\beta = 0$ deg: a) $k_{\zeta_T} = f_{\zeta_T} l_\mu / U_\infty = 0.540$, $\zeta_{T_{\max}} = 3$ deg; b) $k_{\zeta_T} = 0.675$, $\zeta_{T_{\max}} = 3$ deg.

or stationary deflected rudder, the oscillating rudder shifts the rms values of the surface-pressure fluctuations to higher levels (Fig. 11). The rms pressures increase both with rudder frequency and rudder deflection angle even at high angles of attack. The induced shift in rms pressures shows that the potentiality of the commanded auxiliary rudder in diminishing buffet loads can be in the range of 18 to 20%. Also for the oscillating rudder, the pressure spectra show peaked distributions caused by the narrowband fluctuations evoked by the helical mode instability of the breakdown flow (Fig. 12). In addition, spikes occur at the values of the auxiliary rudder frequencies indicating that at these frequencies the fluctuating pressure field is fed with energy. This mechanism is observed for the whole interesting frequency range (Figs. 12a and 12b), substantiating that the actively controlled rudder is efficient to modify the buffet loads. The effectiveness of the auxiliary rudder is caused by aerodynamic and inertial coupling. Inertial coupling increases with frequency, up to the bandwidth of the actuator, whereas aerodynamic effectiveness usually decreases with frequency. Regarding these effects, Fig. 13 shows pressure spectra for both port stations P7, P9, and P11 and starboard stations P8, P10, and P12. All spectra exhibit a peak amplitude at the frequency of the auxiliary rudder oscillation. Because of the increasing impact of the oscillating rudder, the peak values rise in magnitude from leading-edge stations to trailing-edge stations. The comparison of the pressure spectra taken at stations P7 to P12 with those of upper stations P13 (Fig. 12b) to P18 shows that the unsteady pressure at the oscillation frequency is reduced at

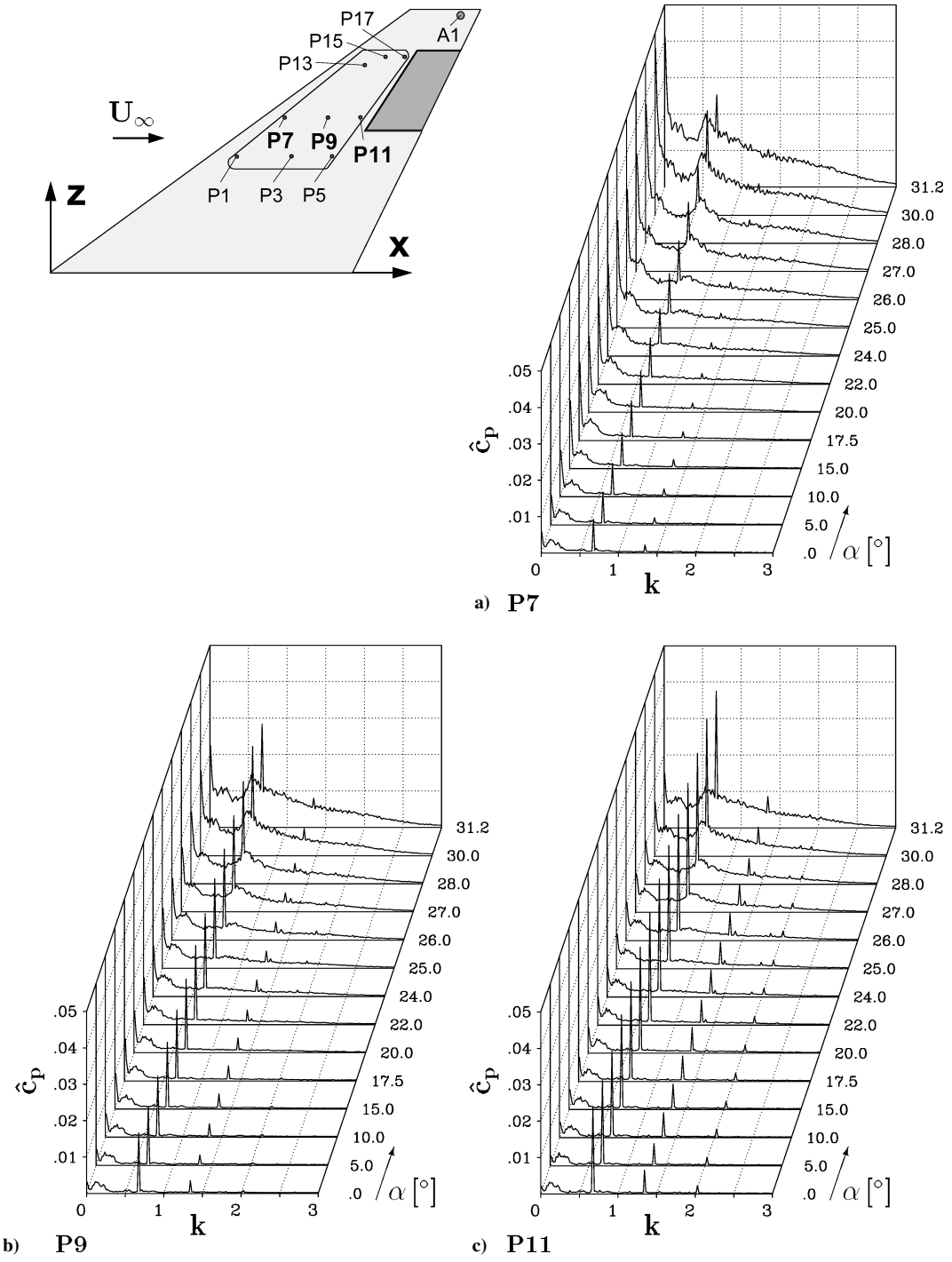

Fig. 13 Amplitude spectra of fin pressure fluctuations $\hat{c}_p$ at port stations a) P7, b) P9, and c) P11, and starboard stations d) P8, e) P10, and f) P12 for all angles of attack tested: $k_{\zeta_T} = 0.675$, and $\zeta_{T_{\max}} = 3$ deg.

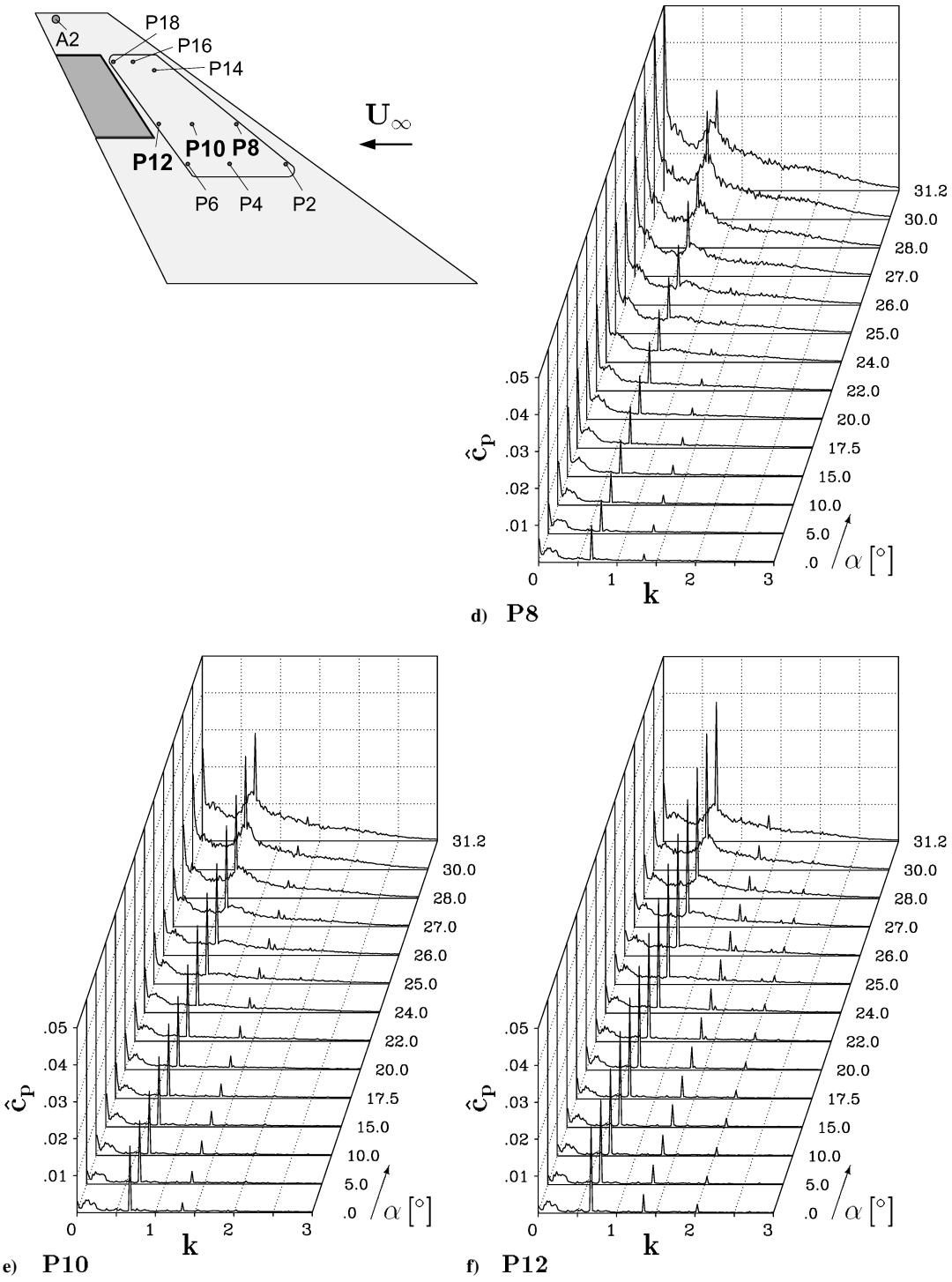

Fig. 13 Amplitude spectra of fin pressure fluctuations $\hat{c}_p$ at port stations a) P7, b) P9, and c) P11, and starboard stations d) P8, e) P10, and f) P12 for all angles of attack tested: $k_{\zeta_T} = 0.675$, and $\zeta_{T_{\max}} = 3$ deg (continued).

stations located closer to the fin root. This reduction is about 38% for leading-edge stations and 34% for trailing-edge stations. Because the modal displacements for lower stations are smaller for the fin first bending mode, the amount of inertial coupling attributed to the rise in unsteady pressure at the oscillation frequency decreases with increasing distance from the fin tip. The remaining part of the motion-induced unsteady pressures is caused by change in circulation as a result of auxiliary rudder oscillations.

Further, amplitudes and phase angles of the first harmonic of the auxiliary rudder moment coefficient are evaluated. The rudder moment coefficient is calculated using dynamic freestream pressure q_∞ and the surface area A_{F_T} and span s_{F_T} of the auxiliary rudder.

$$c_{M_{\zeta_T}} = M_{\zeta_T} \Big/ q_\infty A_{F_T} s_{F_T} \tag{3}$$

It is shown that the amplitude of the rudder moment coefficient $c_{M^A_{\zeta_T}}$ is nearly constant over the considered angle-of-attack range (Fig. 14), demonstrating that there is no reduction of the auxiliary rudder effectiveness at high angle of attack. The phase angle of the auxiliary rudder moment $\Phi_{M_{\zeta_T}}$ with respect to the commanded motion varies between -28 and -42 deg.

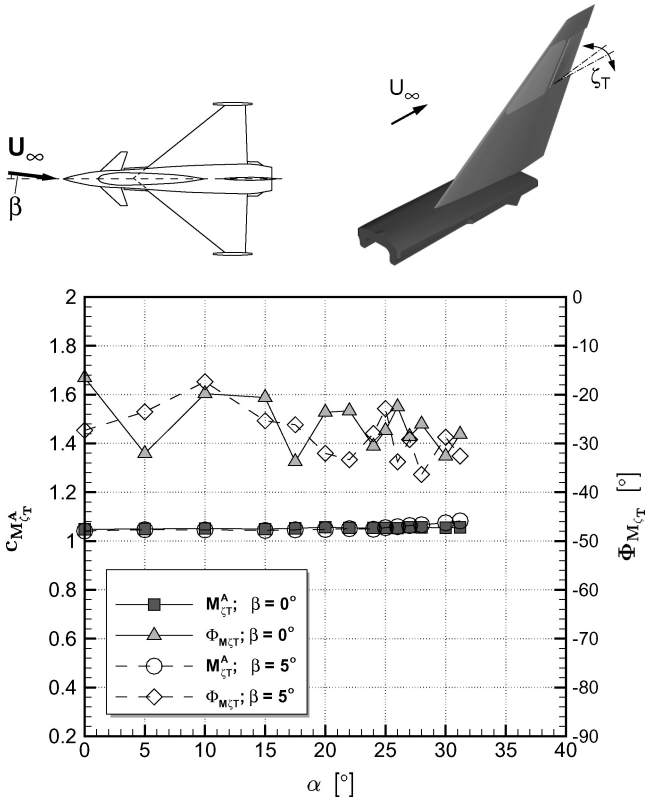

Fig. 14 Amplitude $c_{M^A_{\zeta_T}}$ and phase angle $\Phi_{M_{\zeta_T}}$ of the first harmonic of the auxiliary rudder moment coefficient $c_{M_{\zeta_T}}$ at $k_{\zeta_T} = 0.540$ and $\zeta_{T_{max}} = 3$ deg as function of angle of attack: $U_\infty = 40$ m/s, $Re_{l_\mu} = 0.97 \times 10^6$, $\beta = 0$ and 5 deg.

The open-loop frequency response functions of the fin are calculated using the Fourier-transformed discrete time series of auxiliary rudder deflection angle and fin-tip accelerations. The transfer functions are obtained with the rudder driven harmonically by a linear frequency sweep of $k = 0$ to 0.81 at maximum deflection angles of $\zeta_{T_{max}} = 1$ to 5 deg. To concentrate mainly on the fin first bending mode, the frequency sweep is limited to $k = 0.81$ (90 Hz). Fin-tip accelerations reach a maximum when the rudder oscillates at a reduced frequency of $k = 0.623$ (72.5 Hz) corresponding to half the value of the bending eigenfrequency. Figure 15a shows the amplitude spectrum of the transfer function indicating a dominant peak value at the frequency of the fin first bending mode and some slightly increased values at second-order modes. The associated phase angle function is plotted in Fig. 15b. Because the buffet-induced vibrations contribute to the response of the fin, that is, accelerations in this case, the open-loop frequency response functions are determined for wind-off and wind-on conditions at various angles of attack. The open-loop response functions between the commanded auxiliary rudder deflection angle and the fin-tip accelerations constitute the input-output relationship of the forward loop of the active control system.

Active Buffeting Alleviation

Control Law Synthesis

The components of the active control system include an A/D-converter, a digital controller in which the control law is implemented, and a D/A-converter connected to amplifier and filter elements to operate the actuator and the servomotor, respectively (Fig. 16a). Using the measured open-loop frequency response functions, control laws are designed based on frequency-domain compensation methods.[27] Single-input single-output relationships are applied with the tip accelerometers as sensors to reduce the response in the fin first bending and torsion mode, respectively. The commanded rudder motion can provide damping to alleviate the buffeting of the fin by lagging accelerations by ninety degrees of

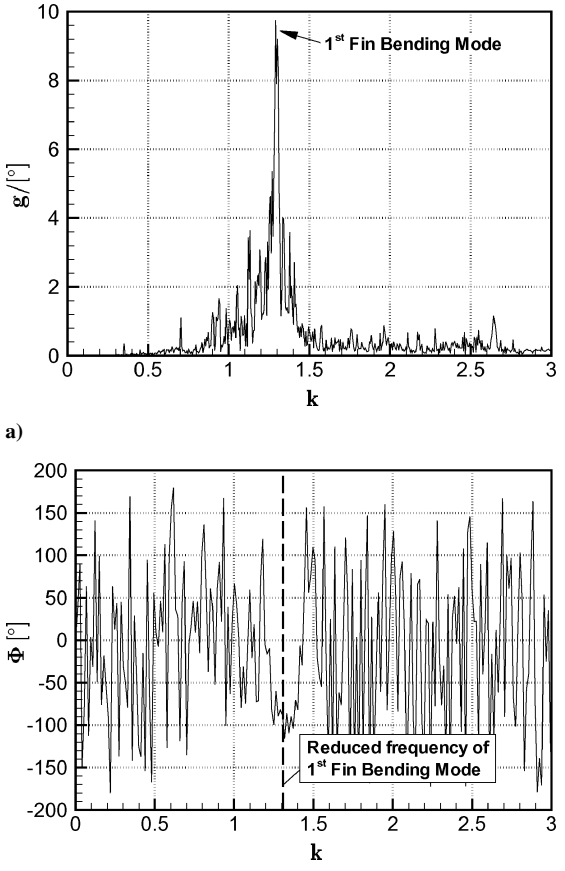

Fig. 15 Open-loop frequency response function of fin-tip accelerations vs commanded auxiliary rudder oscillations for a frequency sweep of $k = 0$ to 0.81 at wind-on and $\alpha = 0$ deg: a) amplitude spectrum and b) phase spectrum.

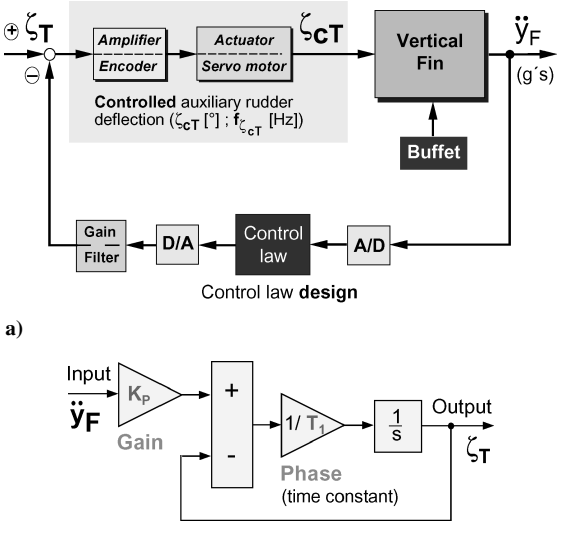

Fig. 16 Schematic of active control system: a) control circuit and b) control law schematic.

phase. Therefore, the baseline control laws are designed to subtract phase at the frequencies of the first eigenmodes so that the actuator phase lags fin-tip accelerations by 90 deg (Fig. 16b). The control law design considers also phase lags associated with the time delays caused by the actuator and gear mechanism as well as by the digital signal processing, especially the controller. Consequently, the control law phase relation is modified by a zero-order hold to take such time delays into account.[27] Avoiding excitation of higher-frequency

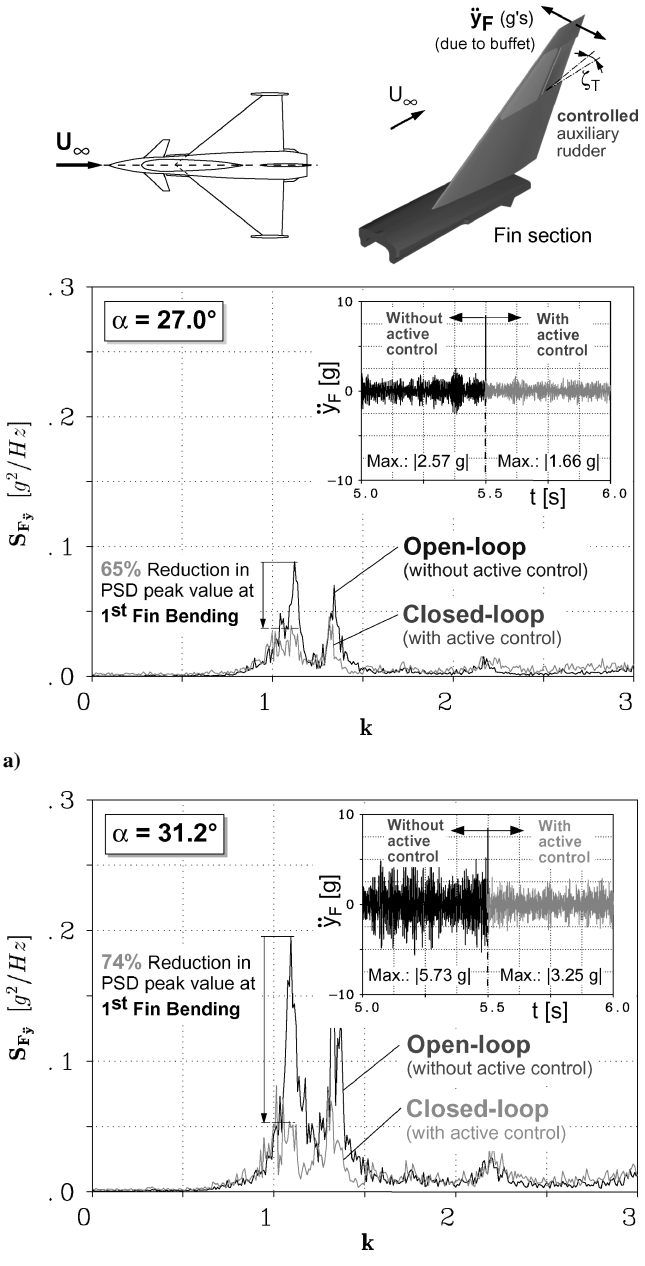

Fig. 17 Comparison of fin-tip acceleration PSDs without and with active control of the first fin bending mode for a) $\alpha = 27$ deg and b) $\alpha = 31.2$ deg: $U_\infty = 40$ m/s, $Re_{l_\mu} = 0.97 \times 10^6$, and $\beta = 0$ deg.

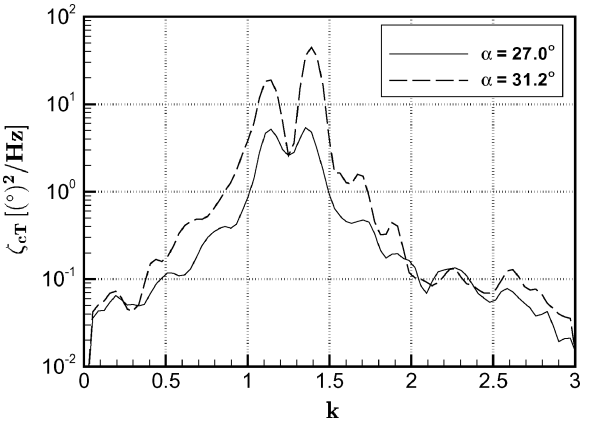

Fig. 18 Power spectral densities of commanded auxiliary rudder deflections for first fin bending mode control.

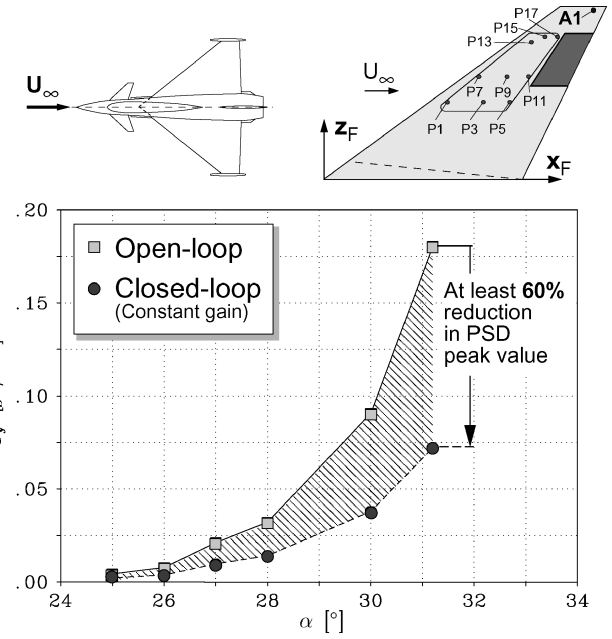

Fig. 19 Comparison of peak values of fin-tip acceleration PSDs without and with active control of the first fin bending mode for various α measured at station A1: $U_\infty = 40$ m/s, $Re_{l_\mu} = 0.97 \times 10^6$, and $\beta = 0$ deg.

modes, sufficient filtering is needed decreasing the control law gain K_p beyond $k \approx 1.4$. Regarding the fin as a single-degree-of-freedom system, the controller performance has been simulated numerically at varying gain settings, and estimates of stability are evaluated.

Active Control Tests

The derived controller parameters are then carefully adapted to run the wind-tunnel tests. As major results, the PSDs of the fin tip accelerations taken at $\alpha = 27.0$ and 31.2 deg are overlayed for open-loop and closed-loop conditions to demonstrate the buffeting alleviation in the first bending mode (Fig. 17). The response of the fin is markedly reduced with a reduction of the PSD peak value of at least 60% while the overall rms value is reduced by approximately 24%. In addition, the corresponding time series exhibit the decrease in the peak values of fin lateral accelerations by applying active control. Corresponding power spectral densities of the commanded auxiliary rudder deflections are depicted in Fig. 18. The reduction in fin-tip accleration PSD peak values for the fin first bending mode of about 60% was achieved with a maximum commanded auxiliary rudder deflection of ±3.6 deg. However, inertia response effects result in a maximum rudder response of ±3.8 to ±4.2 deg. Summarizing, the comparison of the fin-tip acceleration PSD peak values taken without and with active control shows a substantial decrease of the structural dynamic loads related to the first bending mode (Fig. 19). Conducting these tests, a constant gain factor was used over the angle-of-attack range of interest. The significant reduction of the buffet-induced fin-tip accelerations related to the first bending mode is obtained at a gain factor well below the physical limits of the rudder driving system.

Concentrating on the first torsion mode a buffeting reduction can be achieved also. Figure 20 depicts staggered plots of fin-tip acceleration PSDs at several high incidences, $\alpha = 28.0$, 29.0, 30.0, and 31.2 deg. It is shown that with active control the peak values at the frequencies of both the first bending and torsion mode are diminished by as much as 60 to 70%, which substantiates the alleviation potential of the active auxiliary rudder concept. Further improvement in the closed-loop response can be obtained by raising the gain factor in the control law within the stability region without driving the fin first bending or torsion mode, respectively, to increase the percentage of total damping added to the system by using active control. In addition, pressure sensors can be employed to analyze how

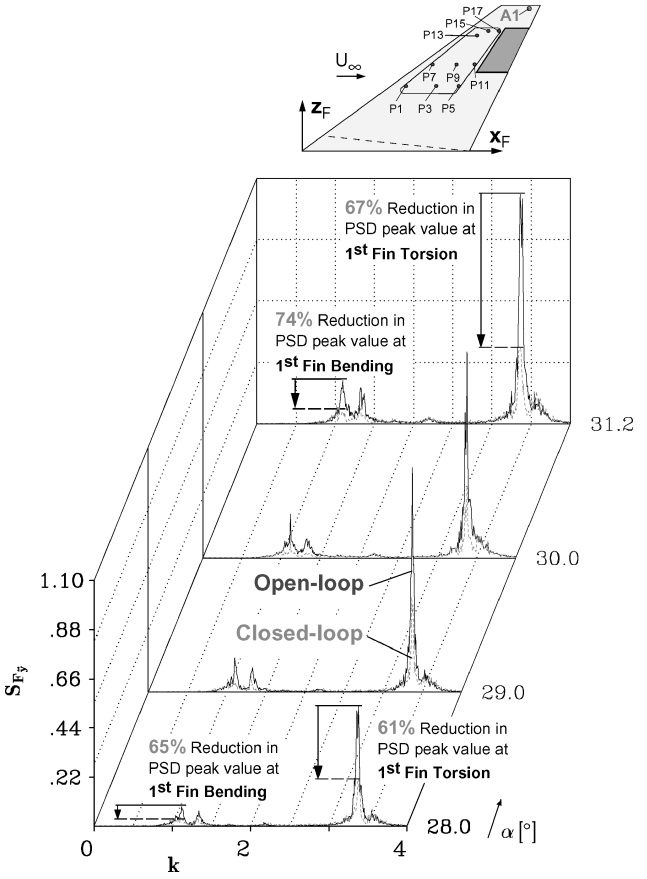

Fig. 20 Comparison of fin-tip acceleration PSDs without and with active control of the first fin bending and torsion mode for various angles of attack: $U_\infty = 40$ m/s, $Re_{l_\mu} = 0.97 \times 10^6$, and $\beta = 0$ deg.

the buffet loads themselves can be further influenced by controlled rudder motions.

Conclusions and Outlook

Experimental investigations have been conducted on active aerodynamic control for fin-buffeting alleviation. A model of a modern fighter aircraft of canard-delta-wing type is used to assess the efficiency of a commanded auxiliary rudder in altering buffet pressures and reducing vibrations in the fin first bending and torsion mode, respectively. A specific fin model featuring an active auxiliary rudder has been fabricated and instrumented to measure unsteady surface pressures, fin-tip accelerations, and transient rudder moment. A digitally controlled servomotor linked to an excenter gear provides harmonic rudder motions at reduced frequencies of $k = 0$ to 0.81 with maximum rudder deflection angle of 5 deg. Wind-tunnel tests at various rudder frequencies and different maximum deflection angles are conducted to quantify the open-loop rudder efficiency at angles of attack up to 31 deg. Control laws based on frequency-domain compensation methods are developed, and the alleviation potential is evaluated. The main results of these investigations are as follows:

1) Vortex bursting associated with a helical mode instability of the breakdown flow is a leading mechanism for inducing severe narrowband pressure fluctuations (buffet) on the fin. The fluctuation levels increase with increasing angle of attack because the fin flow region is affected by characteristic turbulence intensity structures as the burst leading-edge vortices move inboard and upward.

2) Surface-pressure fluctuations induced by harmonic rudder oscillations at open-loop conditions increase with increasing rudder frequency and rudder deflection angle. The corresponding rms pressures are shifted to higher levels even at high angles of attack compared to the levels of the nonoscillating case. Closing the loop, the buffet pressures can be reduced by as much as 18%.

3) The moment amplitude of the driven rudder does not decrease with increasing angle of attack, substantiating the effectiveness of the auxiliary rudder concept also at high α.

4) Single-input single-output control laws are successfully employed to alleviate vibrations (buffeting) in the fin first bending mode and torsion mode, respectively. A constant gain factor corresponding to moderate rudder driving system loads gives satisfactory results at all angles of attack tested.

5) The active control tests show that the peak values of the power spectral densities of the fin-tip accelerations at the fin first bending and torsion mode, respectively, can be reduced by approximately 60% at angles of attack up to 31 deg.

The wind-tunnel tests reported demonstrate active fin-buffeting alleviation on a modern delta-canard high-agility aircraft using a commanded auxiliary rudder. The control system will be further improved by intensively analyzing the parameters of the control law and its stability margins.

Acknowledgments

This work was supported by the EADS GmbH (Military Aircraft). The author would like to thank Dr.-Ing. and J. Becker (EADS MT2) for a long period of fruitful cooperations.

References

[1]Herbst, W. B., "Future Fighter Technologies," *Journal of Aircraft*, Vol. 17, No. 8, 1980, pp. 561–566.

[2]Breitsamter, C., "Turbulente Strömungsstrukturen an Flugzeugkonfigurationen mit Vorderkantenwirbeln," Ph.D. Dissertation, DM 18432, Technische Universität München, Herbert Utz Verlag Wissenschaft (Aerodynamik), Germany, June 1997.

[3]Luber, W., Becker, J., and Sensburg, O., "The Impact of Dynamic Loads on the Design of Military Aircraft," *Loads and Requirements for Military Aircraft*, AGARD-R-815, AGARD, Neuilly Sur Seine, France, 1996, pp. 8-1–8-27.

[4]Del Frate, J. H., and Zuniga, F. A., "In-Flight Flow Field Analysis on the NASA F-18 High Alpha Research Vehicle with Comparisons to Ground Facility Data," AIAA Paper 90-0231, Jan. 1990.

[5]Canbazoglu, S., Lin, J. C., Wolfe, S., and Rockwell, D., "Buffeting of Fins: Distortion of Incident Vortex," *AIAA Journal*, Vol. 33, No. 11, 1995, pp. 2144–2150.

[6]Gursul, I., and Xie, W., "Buffeting Flows over Delta Wings," *AIAA Journal*, Vol. 37, No. 1, 1999, pp. 58–65.

[7]Meyn, L. A., and James, K. D., "Full-Scale Wind Tunnel Studies of F/A-18 Tail Buffet," *Journal of Aircraft*, Vol. 33, No. 3, 1996, pp. 589–595.

[8]Lee, B. H. K., Brown, D., Zgela, M., and Poirel, D., "Wind Tunnel Investigations and Flight Tests of Tail Buffet on the CF-18 Aircraft," *Aircraft Dynamic Loads due to Flow Separation*, AGARD-CP-483, AGARD, Neuilly Sur Seine, France, 1990, pp. 1-1–1-26.

[9]Rizk, Y. M., and Gee, K., "Unsteady Simulation of Viscous Flowfield Around F-18 Aircraft at Large Incidence," *Journal of Aircraft*, Vol. 29, No. 6, 1992, pp. 773–781.

[10]Kandil, O. A., Sheta, E. F., and Liu, C. H., "Computation and Validation of Fluid/Structure Twin Tail Buffet Response," *Euromech Colloquium 349, Simulation of Structure Fluid Interaction in Aeronautics*, German Aerospace Research, Göttingen, Germany, 1996, pp. 15-1–15-10.

[11]Zimmermann, N. H., Ferman, M. A., Yurkovich, R. N., and Gerstenkorn, G., "Prediction of Tail Buffet Loads for Design Applications," AIAA Paper 89-1378, April 1989.

[12]Ferman, M. A., Patel, S. R., Zimmermann, N. H., and Gerstenkorn, G., "A Unified Approach to Buffet Response of Fighter Aircraft Empennage," *Aircraft Dynamic Loads due to Flow Separation*, AGARD-CP-483, AGARD, Neuilly Sur Seine, France, 1990, pp. 1-1–1-26.

[13]Breitsamter, C., and Laschka, B., "Turbulent Flow Structure Associated with Vortex-Induced Fin Buffeting," *Journal of Aircraft*, Vol. 31, No. 4, 1994, pp. 773–781.

[14]Breitsamter, C., and Laschka, B., "Fin Buffet Pressure Evaluation Based on Measured Flowfield Velocities," *Journal of Aircraft*, Vol. 35, No. 5, 1998, pp. 806–815.

[15]Ferman, M. A., Liguore, S. L., Smith, C. M., and Colvin, B. J., "Composite Exoskin Doubler Extends F-15 Vertical Fatigue Life," AIAA Paper 93-1341, April 1993.

[16]Hebbar, S. K., Platzer, M. F., and Frink, W. D., "Effect of Leading-Edge Extension Fences on the Vortex Wake of an F/A-18 Model," *Journal of Aircraft*, Vol. 32, No. 3, 1995, pp. 680–682.

[17]Ashley, H., Rock, S. M., Digumarthi, R. V., Chaney, K., and Eggers, A. J., Jr., "Active Control for Fin Buffet Allevation," U.S. Air Force Wright Lab., WL-TR-93-3099, Wright-Patterson AFB, OH, Jan. 1994.

[18]Hauch, R. M., Jacobs, J. H., Dima, C., and Ravindra, K., "Reduction of Vertical Tail Buffet Response Using Active Control," *Journal of Aircraft*, Vol. 33, No. 3, 1996, pp. 617–622.

[19]Moses, R. W., "Vertical Tail Buffeting Alleviation Using Piezoelectric Actuators—Some Results of the Actively Controlled Response of Buffet-Affected Tails (ACROBAT) Program," Society of Photo-Optical Instrumentation Engineers, Paper 3044, March 1997.

[20]Becker, J., and Luber, W., "Comparison of Piezoelectric and Aerodynamic Systems for Aircraft Vibration Alleviation," Society of Photo-Optical Instrumentation Engineers, Paper 3326-04, March 1998.

[21]Moses, R. W., "Contributions To Active Buffeting Alleviation Programs by the NASA Langley Research Center," AIAA Paper 99-1318, April 1999.

[22]Burnham, J. K., Pitt, D. M., White, E. V., Henderson, D. A., and Moses, R. W., "An Advanced Buffet Load Alleviation System," AIAA Paper 2001-1666, April 2001.

[23]Sheta, E. F., Moses, R. W., Huttsell, L. J., and Harrand, V. J., "Active Control of F/A-18 Vertical Tail Buffeting Using Piezoelectric Actuators," AIAA Paper 2003-1887, April 2003.

[24]Galea, S. C., Ryall, T. G., Henderson, D. A., Moses, R. W., White, E. V., and Zimcik, D. G., "Next Generation Active Buffet Suppression System," AIAA Paper 2003-2905, July 2003.

[25]Sheta, E. F., "Alleviation of Vertical Tail Buffeting of F/A-18 Aircraft," *Journal of Aircraft*, Vol. 41, No. 2, 2004, pp. 322–330.

[26]Breitsamter, C., "Aerodynamic Active Vibration Control For Single-Fin Buffeting Alleviation," *Proceedings of the German Aerospace Congress 1999*, Vol. I, Deutsche Gesellschaft für Luft-und Raumfahrt e. V. (DGLR), Bonn, Germany, 1999, pp. 291–300.

[27]Franklin, G. F., Powel, J. D., and Emami-Naeini, A., *Feedback Control of Dynamic Systems*, Addison Wesley Longman, Reading, MA, 1986.